Toward Protein Structure In Situ: Comparison of Two Bifunctional Rhodamine Adducts of Troponin C

Olivier Julien,* Yin-Biao Sun,† Andrea C. Knowles,‡ Birgit D. Brandmeier,‡ Robert E. Dale,† David R. Trentham,‡ John E. T. Corrie,‡ Brian D. Sykes,* and Malcolm Irving†

*Canadian Institutes of Health Research Group in Protein Structure and Function, Department of Biochemistry, University of Alberta, Edmonton, Canada; †Randall Division of Cell and Molecular Biophysics, King's College London, London, United Kingdom; and ‡MRC National Institute for Medical Research, London, United Kingdom

ABSTRACT As part of a program to develop methods for determining protein structure in situ, sTnC was labeled with a bifunctional rhodamine (BR or BSR), cross-linking residues 56 and 63 of its C-helix. NMR spectroscopy of the N-terminal domain of BSR-labeled sTnC in complex with Ca^{2+} and the troponin I switch peptide (residues 115–131) showed that BSR labeling does not significantly affect the secondary structure of the protein or its dynamics in solution. BR-labeling was previously shown to have no effect on the solution structure of this complex. Isometric force generation in isolated demembranated fibers from rabbit psoas muscle into which BR- or BSR-labeled sTnC had been exchanged showed reduced Ca^{2+}-sensitivity, and this effect was larger with the BSR label. The orientation of rhodamine dipoles with respect to the fiber axis was determined by polarized fluorescence. The mean orientations of the BR and BSR dipoles were almost identical in relaxed muscle, suggesting that both probes accurately report the orientation of the C-helix to which they are attached. The BSR dipole had smaller orientational dispersion, consistent with less flexible linkers between the rhodamine dipole and cysteine-reactive groups.

INTRODUCTION

Fluorescence polarization data from the bifunctional carborhodamine **1** (Fig. 1 *left*) attached to two suitably located cysteine residues on muscle proteins (myosin regulatory light chain and TnC) have been used to study orientations and/or dynamics of the labeled proteins in their native environment in a muscle fiber (1–4). The same rhodamine has been used in single-molecule fluorescence polarization and imaging measurements when attached to one of the calmodulin light chains of myosin V (5,6). Evidence obtained in those studies suggests that the two-site attachment of the BR probe does not alter the native structure or function of the protein. This was supported by an NMR structural study of the N-lobe of the E56C/E63C mutant of sNTnC labeled with $BR\text{-}I_2$ on cysteine residues at positions 56 and 63 of its C-helix, which showed that the labeled protein maintained its native structure (7). In addition, physiological experiments that imply conservation of function are described in several of the above articles. There is thus a body of evidence to suggest that this approach is a reliable and robust way to determine protein and protein domain orientation and motion in situ.

$BR\text{-}I_2$ was deliberately synthesized with flexible arms between the reactive iodoacetamido groups and the fluorophore system (8) in the expectation that it would be able to span cysteines separated over a range of distances. In practice, it has been possible with this reagent to cross-link cysteines located along α-helices, between two helices, and between a helix and a random coil, with separations between their paired Cβ atoms in the range 1.0–1.6 nm (1). A second, commercially available bifunctional sulforhodamine reagent **2** (Fig. 1 *right*) has been used in related fluorescence polarization and single-molecule studies on kinesin (9,10). The ring structure of the linkers between the iodoacetamido groups and the fluorophore in $BSR\text{-}I_2$ is more rigid than the open-chain linkers in $BR\text{-}I_2$, and it might be expected that $BSR\text{-}I_2$ would be less able to accommodate different spacings of the two cysteine residues. In practice, the Cβ distances between cysteines linked by the reagent do span a similar range of distances (1.1–1.6 nm) to those spanned by $BR\text{-}I_2$, but in no case yet described have these pairs of linked residues both been located on the same α-helix. Thus, the residues are either between two helices (N64C and V71C, 1.1 nm), between the end of a β-sheet and a random coil (169C (a native cysteine) and V174C, 1.5 nm), or between

Submitted January 3, 2007, and accepted for publication March 16, 2007.

Oliver Julien and Yin-Biao Sun contributed equally to this work.

Address reprint requests to Malcolm Irving, Randall Division of Cell and Molecular Biophysics, King's College London, London SE1 1UL, United Kingdom. Tel.: 44-207-848-6431; Email: malcolm.irving@kcl.ac.uk.

Abbreviations used: sTnC, chicken skeletal troponin C; TnC, troponin C; sNTnC, N-domain of chicken skeletal troponin C; BR and BSR, bifunctional carborhodamine and bifunctional sulforhodamine moieties, respectively, attached to proteins after two-site labeling with $BR\text{-}I_2$ or $BSR\text{-}I_2$ reagents; Cβ, β-carbon; HPLC, high-performance liquid chromatography; FPLC, fast-protein liquid chromatography; sTnC·BSR1 and sTnC·BSR2 are diastereoisomers that are eluted during preparative HPLC as the first and second peaks of BSR-labeled mutant sTnC; $BSR_{56–63}$, BSR reagent as a mixture of two diastereoisomers attached to cysteines 56 and 63 of mutant sNTnC or sTnC; $TnI_{115–131}$, switch peptide of troponin I; HSQC, heteronuclear single-quantum coherence; $^{15}N\text{-}R_2$, amide transverse relaxation rate; TFA, trifluoroacetic acid.

Editor: David D. Thomas.

0006-3495/07/08/1008/13 $2.00

doi: 10.1529/biophysj.107.103879

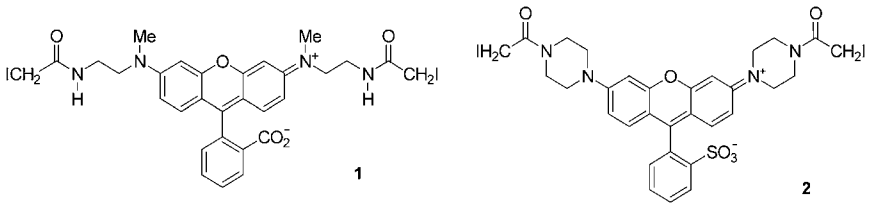

FIGURE 1 Structures of the bifunctional rhodamines **1** (BR-I_2) and **2** (BSR-I_2) used for labeling.

two β-sheets connected by a random coil (T330C and V335C, 1.5 nm) (10). Sequence numbers and distances are from the rat kinesin structure (pdb 2kin). The 169–174 Cβ distance in human kinesin (pdb 1bg2) is slightly longer (1.6 nm) (9).

To date, there have been no published studies comparing the efficacy of BSR-I_2 and BR-I_2 for determining the in situ orientation of the vector joining the same pair of target cysteines. The ideal bifunctional probe reagent for this type of in situ structural measurement would have three key properties: 1), efficient cross-linking of a suitably placed pair of cysteine residues in a target protein domain; 2), no alteration of the native structure and function of the target domain as a result of such cross-linking; and 3), accurate reporting of the in situ orientation of the vector joining the two cysteines to which the probe is attached. These properties may be to some extent mutually exclusive. For example, flexible linkers between probe and protein may be desirable with respect to the first two properties, but detrimental to the third. Moreover, the third property cannot in general be assessed directly in the absence of alternative techniques that can determine the orientation of the cysteine-cysteine vector in situ. In these circumstances, the most powerful available approach is to compare the orientations of different probes attached to the same pair of cysteines and the structural and functional properties of the different labeled proteins.

In this work, we labeled the C-helix of sNTnC separately with BR-I_2 or BSR-I_2 via its E56C/E63C mutant, in which the β-carbon atoms of the two cysteines are ~1.1 nm apart. We used a kinetic competition experiment to determine the relative chemical reactivity of the two reagents. We studied BSR-labeled sNTnC in complex with Ca^{2+} and $TnI_{115–131}$ by NMR for comparison with the published structure of the corresponding BR-labeled complex (7). We labeled the same C-helix residues of whole sTnC with either BR-I_2 or BSR-I_2, exchanged the labeled proteins into permeabilized muscle fibers, and determined the effect of each probe on active force generation and its regulation by Ca^{2+}. Finally, we measured the in situ orientation and mobility of both the BR and BSR probes, using a novel analytic approach to determine these parameters from the polarized fluorescence intensities.

MATERIALS AND METHODS

Chemicals and biochemicals

BR-I_2 was prepared as described previously (8) and BSR-I_2 was purchased from Molecular Probes (Eugene, OR). The double-cysteine (E56C and E63C) mutant sNTnC, isotopically labeled with ^{13}C and ^{15}N, was expressed and purified as described previously (7). The isotopic enrichment, estimated from mass spectrometry, was ~95% for ^{13}C and ~93% for ^{15}N. The full-length E56C/E63C/C101A mutant chicken skeletal troponin C, and the same protein labeled with BR-I_2, were prepared as previously described (3). Chemical constituents for the solutions used in the muscle fiber experiments were obtained from Sigma (Poole, Dorset, U.K.) except where noted otherwise.

Labeling of E56C/E63C-mutant sNTnC with BSR-I_2

A solution of 8 mg sNTnC at 1 mg/ml in labeling buffer (25 mM Tris/HCl, 100 mM NaCl, 1 mM $MgCl_2$, pH 7.4) was incubated overnight on ice with 2 mM dithiothreitol (final concentration) to reduce disulfides that formed during storage. Reduction was monitored by reverse-phase HPLC ((C18 VYDAC column, 218TP54; guard column, 218GCC54, Grace Vydac, Columbia, MD), eluting at 1 ml/min with a linear gradient of 60% solvent A (H_2O, 0.1% TFA) and 40% solvent B (acetonitrile, 0.082% TFA) to 40% solvent A and 60% solvent B over 20 min), and was characterized by a change from an initially complex elution profile to a principal species that eluted at 52.3% solvent B. The protein was then gel-filtered using PD-10 columns (GE Healthcare, Chalfont St. Giles, U.K.), which were equilibrated with labeling buffer that also contained 52.5 μM tris(carboxyethyl)phosphine. After elution, the protein was diluted to a concentration of 0.55 mg/ml (52.5 μM) using the same buffer. BSR-I_2 was then added (final concentration, 105 μM) from a 25 mM stock solution in dimethylformamide. The reaction mixture was incubated in the dark at 20°C for 40 min and the course of the reaction was monitored (after quenching an aliquot with 2-mercaptoethanesulfonate (see below)) by analytical reverse-phase HPLC as specified above. Protein elution was monitored by absorbance at 215 nm and by rhodamine fluorescence (λ_{ex} 549 nm, λ_{em} >580 nm). sNTnC in which both cysteines had been cross-linked by BSR (i.e., the desired product) eluted as a double peak at 50.3% and 51.1% solvent B. Unreacted sNTnC eluted at 52.3% solvent B, as above. All assignments were made retrospectively, after analysis of fractions by electrospray mass spectrometry. We did not seek to identify material in other fractions, which may have contained species labeled with two BSR moieties. After the 40-min incubation, the labeling reaction was quenched with sodium 2-mercaptoethanesulfonate (final concentration, 3.4 mM) and kept in the dark for a further 30 min at 20°C. Aliquots of the solution were filtered through PD-10 columns (2.5 ml per column) into FPLC buffer (10 mM potassium phosphate, 1 mM $MgCl_2$, pH 7.5) to remove unconjugated rhodamine. The labeled sNTnC (0.31 mg/ml) was purified at 4°C on a 16/10 Mono-Q ion exchange column (GE Healthcare), using a linear gradient of 0.25–0.35 M NaCl in FPLC buffer at a flow rate of 2 ml/min. The protein eluted as two peaks with near-baseline resolution at 0.31 M and 0.32 M NaCl. One-milliliter fractions were collected and assayed for purity by analytical HPLC (as above) and electrospray mass spectrometry (measured mass for each peak, 11005.6 ± 1.8 Da). Fractions containing both peaks of the pure sNTnC·$BSR_{56–63}$ (>90% homogeneity) were pooled and dialyzed against 10 mM KCl, 0.42 mM $CaCl_2$ (2 × 5 L, each for 2 h, then 1 × 3 L overnight, all at 4°C). The contents of the dialysis bag (2 ml) were then concentrated to 1 ml using a Vivaspin 20 concentrator (Vivascience, Epsom, U.K.) at 1140 × g. The concentrated solution of labeled protein (1.04 mg/ml, based on an extinction coefficient of 52,000 M^{-1} cm^{-1} at 528 nm (3)) was flash frozen in liquid nitrogen and stored at −20°C.

Labeling of E56C/E63C/C101A-mutant sTnC with BSR-I_2

Labeling of full-length sTnC with BSR-I_2 was performed by a protocol similar to that previously described for BR-I_2 (3). HPLC analysis was as described above. sTnC·$BSR_{56–63}$ eluted as a partly resolved double peak at ~53.0% and 53.3% acetonitrile. The species in each peak had the same mass (±1 Da). The labeled protein was purified in 1-mg aliquots on a C4 VYDAC 214TP510 column with a linear gradient from 60% solvent A (H_2O, 0.1% TFA) and 40% solvent B (acetonitrile, 0.082% TFA) to 40% solvent A and 60% solvent B, run at 2 ml/min over 1 h. The two peaks, containing the separate diastereoisomers of the labeled protein and referred to as sTnC·BSR1 and sTnC·BSR2, were collected manually and immediately stored on ice. The combined fractions of each peak were dialyzed as soon as practicable into 10 mM Tris/HCl, 1 mM $MgCl_2$, 100 mM NaCl, pH 7.5 (each 2 × 5 L for 2 h, then 1 × 5 L overnight, all at 4°C). The dialysis bag was placed on a bed of solid sucrose and concentrated to a final protein concentration of 1–2 mg/ml. The labeled protein was flash frozen in liquid nitrogen and stored at −80°C.

Competitive C-helix labeling with BR-I_2 and BSR-I_2

A 50-μM solution of reduced mutant sTnC in labeling buffer (as above) was treated with a dimethylformamide solution of BR-I_2 and BSR-I_2 (final concentrations, 100 μM each) and incubated for 40 min at 20°C. Unreacted rhodamines were quenched by addition of sodium 2-mercaptoethanesulfonate (final concentration, 6 mM) and, after 40-min incubation at 20°C, unconjugated rhodamine was removed by gel filtration in labeling buffer (PD-10 column). The eluted protein mixture was analyzed by electrospray mass spectrometry.

NMR sample preparation

One ml of the solution prepared above of 1.04 mg/ml {^{13}C,^{15}N}-sNTnC·$BSR_{56–63}$ in 0.42 mM $CaCl_2$ and 10 mM KCl was concentrated by centrifugation at 5000 × *g* using Centricon YM-10 tubes (Millipore, Billerica, MA). To this solution were added 5 μl of 10 mM 2,2-dimethyl-2-silapentane-5-sulfonic acid and 5 μl of 100 mM imidazole in D_2O. Afterward, 50 μl D_2O was added to obtain a volume of 500 μl in 90% H_2O/10% D_2O. The pH was adjusted to 6.78 (using 1 M HCl) by following the imidazole peak in the 1D NMR spectrum (11). The final protein concentration was 0.1 mM (by amino acid analysis) in 20 mM KCl. The salt concentration was kept as low as possible to obtain better results using a spectrometer equipped with a cryogenic probe. Later, 0.4 mg $TnI_{115–131}$ (Ac-RMSADAMLKALLGSKHK-NH_2) was added to the sample. The pH dropped to 5.98 and was readjusted to 6.62 using 1 M NaOH. The complex so formed is referred to as sNTnC·$2Ca^{2+}$·$TnI_{115–131}$·$BSR_{56–63}$.

NMR spectroscopy

All NMR spectra were acquired on Varian INOVA 600-MHz and 800-MHz spectrometers (the latter equipped with a cryogenic probe) using BioPack pulse sequences (Varian, Palo Alto, CA). A two-dimensional {^{1}H-^{15}N}-HSQC spectrum was collected at 800 MHz with 1024 (^{1}H) × 512 (^{15}N) complex points, 32 transients, and spectral widths of 11,990 Hz and 3242 Hz for the first and second dimensions, respectively. For better digital resolution in the ^{13}C-dimension, the 3D spectra were acquired at 600 MHz. A 3D CBCA(CO)NH spectrum was acquired with 1024 (^{1}H) × 128 (^{13}C) × 64 (^{15}N) complex points and 24 transients. On the same spectrometer, a 3D HNCACB spectrum was collected with 1024 (^{1}H) × 128 (^{13}C) × 64 (^{15}N) complex points and 32 transients. The spectral width for the 3D spectra was 8398 Hz in the ^{1}H-dimension, 2431 Hz in the ^{15}N-dimension, and 12,068 Hz in the ^{13}C-dimension. All spectra were acquired at 30°C.

To calculate a per residue backbone amide ^{15}N transverse relaxation rate, a set of six 2D {^{1}H-^{15}N}-HSQC spectra were acquired at 600 MHz with different relaxation time delays (τ = 10, 30, 50, 70, 90, and 110 ms). Spectra were collected with 1024 (^{1}H) × 512 (^{15}N) complex points, 32 transients, an equilibrium delay of 3.5 s, and spectral widths of 11,990 Hz and 3242 Hz. The relaxation rate per residue was calculated with the Rate Analysis function of NMRView 5.0.4 (12) for all assigned peaks of the HSQC spectrum, except for those peaks showing strong overlap (to avoid integration of two resonances into one).

The spectra were processed using NMRPipe (13). In general, a sine-bell function shifted by 60° or 90° was applied to the free induction decays, after a linear prediction limited in length to half the number of experimental points collected. The free induction decays were zero-filled with a maximum of twice the number of complex points acquired before analysis with NMRView and Smartnotebook (14). The secondary structure prediction based on a Cα chemical shifts homology was performed using the program Chemical Shift Index (15).

Muscle fibers and solutions

All solutions used in muscle fiber experiments contained 25 mM imidazole, 5 mM MgATP, 1 mM free Mg^{2+} (added as magnesium acetate) and 10 mM EGTA, with the exception of preactivating solution, which had 0.2 mM EGTA. Ionic strength was adjusted to 150 mM by addition of potassium propionate (KPr), and the pH was 7.1 at 10°C. Ca^{2+} concentration (expressed as pCa, the negative $\log_{10}$ of the molar value) was adjusted by varying the relative amounts of K_2EGTA and CaEGTA, keeping total [EGTA] at 10 mM in all solutions except the preactivating solution. No CaEGTA was added to the relaxing solution (pCa 9). TnC-extraction solution contained 0.5 mM trifluoperazine (Fluka, Poole, U.K.), 20 mM MOPS, 5 mM EDTA, and 130 mM KPr, pH 7.1, at 10°C.

Adult New Zealand white rabbits were killed by sodium pentobarbitone injection (200 mg kg^{-1}). Small fiber bundles were dissected from the psoas muscle, demembranated, and stored for up to 4 weeks in relaxing solution containing 50% (v/v) glycerol at −20°C (16). Single fiber segments 2.5–3.5 mm long were dissected in the above storage solution on a cooled microscope stage and mounted, via aluminum T-clips, at sarcomere length 2.4 μm between a force transducer (AE801, Memscap, Bernin, France) and a fixed hook in a 60-μl glass trough containing relaxing solution. The experimental temperature was 10.0 ± 0.5°C.

TnC extraction and reconstitution

Native TnC was selectively extracted from single glycerinated rabbit psoas muscle fibers by repeated 30-s incubations in TnC-extraction solution followed by 30 s in relaxing solution. After a total of 20 such cycles, no Ca^{2+}-activated force could be detected at pCa 4.5. Fibers were reconstituted with labeled sTnC by bathing them in relaxing solution containing ~1.0 mg/ml labeled sTnC for 60 min at 10°C.

Fluorescence polarization and physiological measurements

Force and polarized fluorescence intensities from BR- or BSR-labeled sTnC were measured as described (17). The central 1.5-mm segment of a fiber mounted horizontally in a temperature-controlled trough was briefly illuminated from below with 532 nm light polarized either parallel or perpendicular to the fiber axis. The fluorescent light emitted from the fiber and propagating in the vertical direction (in line with the illuminating beam) was collected by a 10× 0.3 NA objective (Plan Fluor, Nikon, Tokyo, Japan). A similar objective collected fluorescence in the horizontal direction (at 90° to both illuminating beam and fiber axis). In each channel, the fluorescence was selected by a 610-nm filter with 75-nm bandpass, and separated into parallel

and perpendicular components by a Wollaston prism. The resultant polarized fluorescence intensities were measured simultaneously by four photomultipliers (R4632, Hamamatsu, Hamamatsu City, Japan) for each excitation polarization. Relative transmittances of the excitation and emission channels and photomultiplier sensitivities were measured using an isotropic film of rhodamine in polyvinylalcohol sandwiched between two 45° prisms (18), and appropriate correction factors applied to the fiber data. Three independent order parameters, $\langle P_{2d}\rangle$, $\langle P_2\rangle$, and $\langle P_4\rangle$, were calculated from the eight corrected intensities (19). The orientation of the BR and BSR dipoles with respect to the fiber axis, averaged over timescales that are long compared with the lifetime of the excited state, was estimated from $\langle P_2\rangle$ and $\langle P_4\rangle$, by fitting model orientation distributions with a Gaussian shape (3), and by maximum entropy analysis (20). Each pair of $\langle P_2\rangle$ and $\langle P_4\rangle$ values was fitted by a Gaussian orientation distribution with peak angle θ_g and standard deviation σ according to the formulae

$$\langle P_2\rangle = \frac{\int_{-\pi/2}^{\pi} P_2(\cos\theta)\exp\left[-(\theta-\theta_g)^2/2\sigma^2\right]d\theta}{\int_{-\pi/2}^{\pi}\exp\left[-(\theta-\theta_g)^2/2\sigma^2\right]d\theta}$$

and

$$\langle P_4\rangle = \frac{\int_{-\pi/2}^{\pi} P_4(\cos\theta)\exp\left[-(\theta-\theta_g)^2/2\sigma^2\right]d\theta}{\int_{-\pi/2}^{\pi}\exp\left[-(\theta-\theta_g)^2/2\sigma^2\right]d\theta}$$

where the integration limits are chosen to include the possible contribution of tails of the Gaussian distribution outside the region $0 < \theta < \pi/2$ when θ_g is within that range, $P_2(\cos\theta)$ is the function $0.5(3\cos^2\theta - 1)$, and $P_4(\cos\theta)$ is $0.125(35\cos^4\theta - 30\cos^2\theta + 3)$. Note that no $\sin\theta$ weighting terms are included in the integrals. This model, in contrast with those used previously (1–3), corresponds to a Gaussian distribution of axial angles of the probe molecules at each azimuth without truncation at the quadrant boundaries. The symmetries of the muscle fiber structure, the cylindrical symmetry around the fiber axis combined with the bipolar organization of sarcomeres and the dipole nature of the probes, converts the Gaussian distribution in the molecular coordinate frame into a ''folded Gaussian'' distribution in the fiber coordinate frame by effectively reflecting the $\theta < 0$ and $\theta > \pi/2$ tails into the region $0 < \theta < \pi/2$. The mean angle (θ_f) of this folded Gaussian distribution in the range $0 < \theta < \pi/2$ will, in general, not be equal to θ_g.

The maximum entropy distribution f_{ME} of the angle θ between the probe dipole and the fiber axis is the broadest distribution that is consistent with the measured $\langle P_2\rangle$ and $\langle P_4\rangle$ values, calculated to maximize the informational entropy of the distribution defined as $-\int_0^{\pi} f_{ME}\ln(f_{ME})d\theta$. Again there is no $\sin\theta$ weighting in the integral, in contrast with the previous formulation (20), so here f_{ME} represents the maximum entropy estimate of the total number of probes at angle θ, independent of space-filling or other assumptions related to the azimuthal distribution of probe dipoles in the cylindrically symmetrical coordinate system of the fiber. f_{ME} is proportional to $\exp[\lambda_2 P_2(\cos\theta) + \lambda_4 P_4(\cos\theta)]$, where λ_2 and λ_4 are Lagrange multipliers, chosen to fit the measured $\langle P_2\rangle$ and $\langle P_4\rangle$ values using the equations

$$\langle P_2\rangle = \frac{\int_0^{\pi} P_2(\cos\theta)\exp\left[\lambda_2 P_2(\cos\theta) + \lambda_4 P_4(\cos\theta)\right]d\theta}{\int_0^{\pi}\exp\left[\lambda_2 P_2(\cos\theta) + \lambda_4 P_4(\cos\theta)\right]d\theta}$$

and

$$\langle P_4\rangle = \frac{\int_0^{\pi} P_4(\cos\theta)\exp\left[\lambda_2 P_2(\cos\theta) + \lambda_4 P_4(\cos\theta)\right]d\theta}{\int_0^{\pi}\exp\left[\lambda_2 P_2(\cos\theta) + \lambda_4 P_4(\cos\theta)\right]d\theta}.$$

The mean of the f_{ME} distribution in the range 0 to $\pi/2$, θ_{ME}, was calculated as

$$\int_0^{\pi/2}\theta f_{ME}d\theta \Big/ \int_0^{\pi/2} f_{ME}d\theta.$$

Force and polarized fluorescence data were measured during a series of activations at different $[Ca^{2+}]$ in each fiber. Each activation was preceded by a 1-min incubation in preactivating solution and followed by a 5-min incubation in relaxing solution. Force and polarized fluorescence intensities were measured after a steady force had been established in each activation. Maximum isometric force at pCa 4.5 was recorded before and after each series of activations at submaximal $[Ca^{2+}]$; if maximum isometric force had decreased by >10%, the fiber was discarded. The dependence of force and of order parameters on $[Ca^{2+}]$ for each fiber were fitted using least-squares regression to the Hill equation:

$$Y = 1/(1 + 10^{n_H(pCa - pCa_{50})}),$$

where pCa_{50} is the pCa corresponding to half-maximal change in the parameter Y, and n_H is the Hill coefficient specifying the steepness of the Ca^{2+}-dependence. Force-pCa relationships were described by expressing submaximal Ca^{2+}-activated force at each pCa as a fraction of maximum Ca^{2+}-activated force determined at pCa 4.5.

RESULTS

Diastereoisomers of labeled proteins

As previously described for the same proteins labeled with BR-I_2 (3,7), the BSR-labeled N-lobe and full-length proteins were produced as a mixture of diastereoisomers. This occurs because there is a barrier to rotation about the bond that joins either the carboxylated or sulfonated phenyl ring to the three coplanar rings that comprise the fluorophore of these rhodamine dyes (Fig. 1). Quantum mechanics calculations indicate a value of ~27 kcal/mol for this rotational barrier (21). Although the diastereoisomers in this case for the labeled sNTnC were resolved by both HPLC and FPLC, they were recombined after purification because of the small amount of protein available.

Relative reactivity of BR-I_2 and BSR-I_2

Mass spectrometric analysis (Fig. 2) of the unfractionated mixture of products obtained after incubation of the mutant sTnC with a mixture of BR-I_2 and BSR-I_2 (each rhodamine in twofold molar concentration with respect to that of the protein) showed the predominant presence of one labeled species, identified as sTnC·BSR. The calculated molecular weights of the various species, from which the structural assignments were made, are given in the figure legend. sTnC·BR was barely detectable in the unfractionated mixture, and other minor components identified had two rhodamines attached to the protein. The predominance of sTnC·BSR in the product mix shows that BSR-I_2 reacts more rapidly than BR-I_2 with the thiol groups of the mutant sTnC.

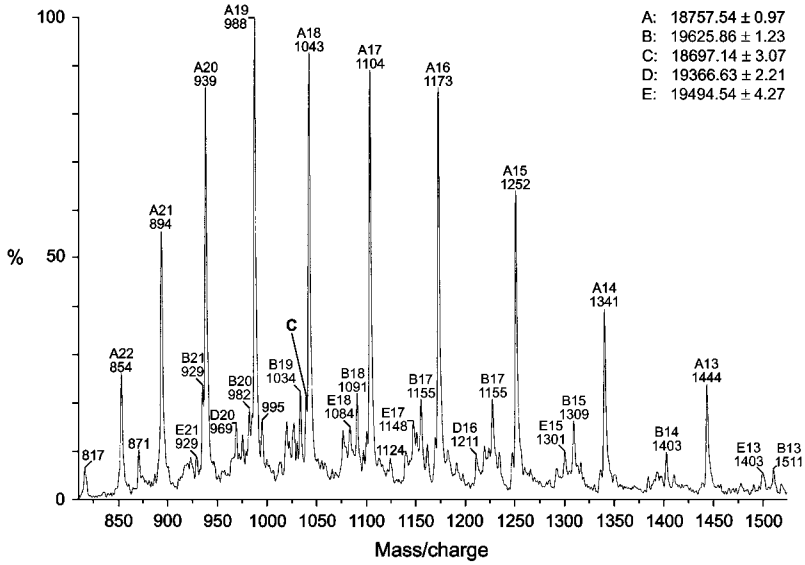

FIGURE 2 Electrospray mass spectrum of the unfractionated E56C/E63C/C101A sTnC mutant after competitive labeling with a mixture of BR-I_2 and BSR-I_2. The major series (A-peaks) corresponds to the expected mass of sTnC·BSR (calculated mass, 18,757.4 Da). The single peak marked C is the only one resolved that corresponds to sTnC·BR (calculated mass, 18,697.3 Da). Of the remaining species (B, D, and E), two correspond to TnC labeled with two rhodamine moieties. B is from TnC carrying two BSR moieties, with the iodoacetamide functions on their distal ends both displaced by 2-mercaptoethanesulfonate (calculated mass, 19,624.5 Da). E represents double labeling by BR, but with only one of the iodoacetamides on the side chains not attached to cysteine residues displaced by 2-mercaptoethanesulfonate (calculated mass, 19,491.0 Da). The exact nature of species D could not be assigned.

Backbone chemical shift comparison between sNTnC·2Ca^{2+}·TnI$_{115–131}$·BSR$_{56–63}$ and sNTnC·2Ca^{2+}·TnI$_{115–131}$·BR$_{56–63}$

Even with only 1 mg of {^{13}C,^{15}N}-sNTnC·2Ca^{2+}·TnI$_{115–131}$·BSR$_{56–63}$, high quality NMR spectra could be obtained using an 800-MHz spectrometer equipped with a cryogenic probe. A portion of the 2D {^{1}H-^{15}N}-HSQC NMR spectrum is shown in Fig. 3. sNTnC·2Ca^{2+}·TnI$_{115–131}$·BR$_{56–63}$ was previously found to undergo partial dimerization in solution, with the proportion of dimer decreasing at higher salt concentrations (7). To evaluate the monomer/dimer ratio for sNTnC·2Ca^{2+}·BSR$_{56–63}$ under the conditions of this experiment, the ^{15}N-R_2 of sNTnC·2Ca^{2+}·BSR$_{56–63}$ was measured at 600 MHz before adding TnI$_{115–131}$. A relaxation rate of 9.6 s^{-1} was obtained from the decay of the amide envelope using the 1D trace of the first increment of six {^{1}H-^{15}N}-HSQC spectra with different time delays (see Materials and Methods). This relaxation experiment reflects the apparent molecular weight of sNTnC·2Ca^{2+}·BSR$_{56–63}$, and consequently estimates the monomer/dimer ratio in solution. The ^{15}N-R_2 value measured at 20 mM KCl was equivalent to that obtained by Mercier et al. (7) for sNTnC·2Ca^{2+}·TnI$_{115–131}$·BR$_{56–63}$ at 320 mM KCl ($R_2 = 9.8$ s^{-1}), which indicates that sNTnC·2Ca^{2+}·BSR$_{56–63}$ has little tendency to dimerize at the concentration used. As a result, no more salt was added, as it would have compromised acquisition of NMR spectra on the 800-MHz NMR spectrometer. The subsequent addition of TnI$_{115–131}$ to form the final complex further reduces the tendency to dimerize (22).

The backbone NMR chemical shift assignments were carried out from a 2D {^{1}H-^{15}N}-HSQC spectrum for the amides, and 3D HNCACB and 3D CBCA(CO)NH spectra for the Cα and Cβ nuclei using Smartnotebook (14). The backbone assignment of sNTnC in the sNTnC·2Ca^{2+}·TnI$_{115–131}$·BSR$_{56–63}$ complex was completed to 97.7% (N, HN, Cα and Cβ). The only missing atoms are the Cβ of residues 57 and 61. As noted above, two diastereoisomers were generated during the labeling of sNTnC with BSR-I_2. As a result, twin peaks were observable for several residues in the HSQC spectrum (Fig. 3). Twinning was clearly identifiable for residues 54, 56, 58, 59, and 60, situated close to the BSR probe on the C-helix. The peak with higher intensity was chosen for the backbone assignment, but relaxation rates were determined for both peaks. These five residues were identified according to the size of the chemical shift difference between the two resonances, the presence of separate Cα and Cβ resonances in 3D spectra, and the relative peak intensity of the corresponding peaks (approximately equal) in 2D and 3D spectra. Other resonances appearing as major and minor peaks (e.g., residues 8, 10, 23, 39, and 73) could result from the presence of the two diastereoisomers, or could come from another phenomenon like the monomer-dimer equilibrium existing in solution.

The backbone chemical shifts of sNTnC·2Ca^{2+}·TnI$_{115–131}$·BSR$_{56–63}$ were compared to sNTnC·2Ca^{2+}·TnI$_{115–131}$·BR$_{56–63}$ for all assigned atoms (Fig. 4). The overall backbone chemical shifts did not reveal significant changes. On average, the difference of chemical shifts between the two N-domains is 0.26 ppm for the N nuclei, 0.04 ppm for the amide protons, 0.12 ppm for the Cα nuclei, and 0.13 ppm for the Cβ nuclei. The maximum deviations observed for the HN (0.28 ppm), N (0.78 ppm), Cα (0.76 ppm), and Cβ (0.67 ppm) reflect this high level of similarity. More importantly, the chemical shifts observed for the residues from E56C to E63C do not show significantly higher variation than residues in the rest of the protein, which indicates that the C-helix is not perturbed by the presence of this more rigid probe. Moreover, the secondary structure prediction based on Cα chemical shift homology shows the presence of the α-helices and β-sheets in the same positions as for sNTnC·2Ca^{2+}·TnI$_{115–131}$·BR$_{56–63}$

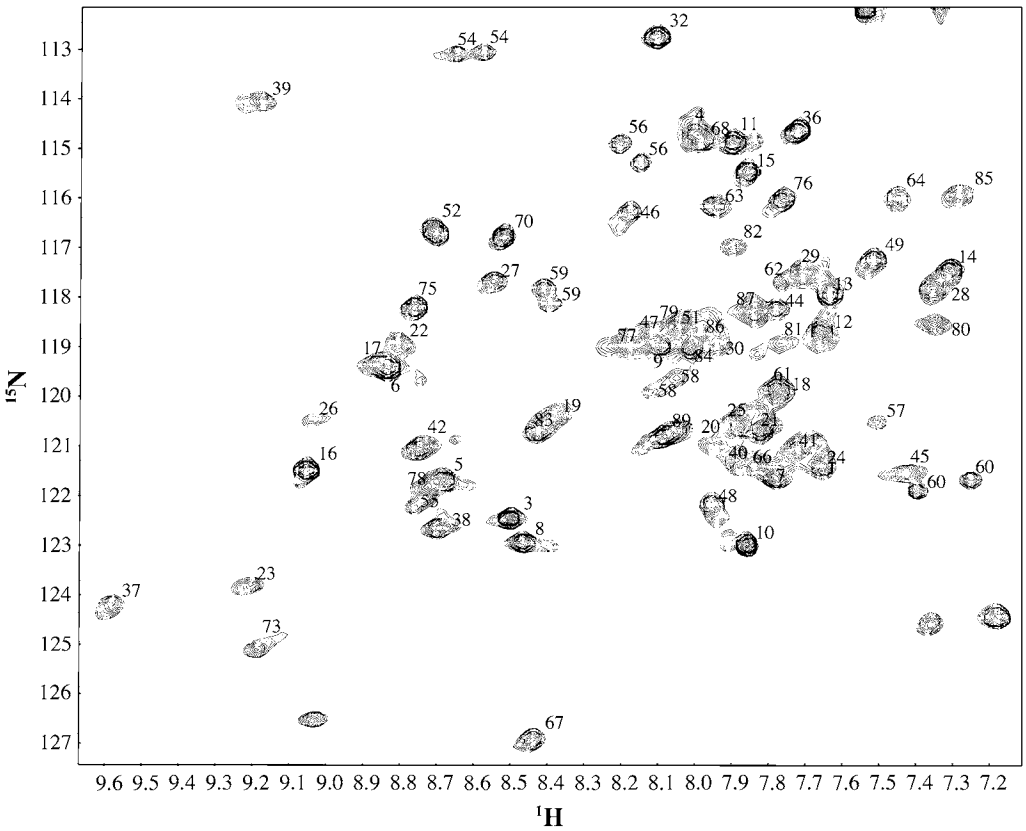

FIGURE 3 Selected region of the 2D $\{^1H\text{-}^{15}N\}$-HSQC NMR spectrum of sNTnC·2Ca^{2+}·TnI$_{115–131}$·BSR$_{56–63}$ acquired at 800 MHz using a cryogenic probe. Twin peaks are clearly observed for residues 54, 56, 58, 59, and 60, reflecting the presence of two diastereoisomers in solution.

(Fig. 5). The prediction indicates a secondary structure of sNTnC·2Ca^{2+}·TnI$_{115–131}$·BSR$_{56–63}$ essentially identical to that of sNTnC·2Ca^{2+}·TnI$_{115–131}$·BR$_{56–63}$ for the well-defined regions (residues 3–85), and a perfect match for the C-helix.

Transverse relaxation measurement of sNTnC·2Ca^{2+}·TnI$_{115–131}$·BSR$_{56–63}$

Having demonstrated that the C-helix is intact, we used amide ^{15}N relaxation data to probe the mobility of residues in the protein. The ^{15}N relaxation rates of sNTnC in the sNTnC·2Ca^{2+}·TnI$_{115–131}$·BSR$_{56–63}$ complex were determined on a per residue basis (Fig. 6). The average ^{15}N-R_2 obtained was 11.6 ± 2.8 s^{-1} using every nonoverlapping residue (80 peaks). This relaxation rate is higher than the value given here for sNTnC·2Ca^{2+}·BSR$_{56–63}$, since TnI$_{115–131}$ is bound to the N-domain and forms a higher molecular weight complex. The expected ^{15}N-R_2 values for sNTnC·2Ca^{2+}·TnI$_{115–131}$·BSR$_{56–63}$ are ~9 s^{-1} for a monomer and ~18 s^{-1} for a dimer. These were determined from the correlation between the relaxation rates of different TnC complexes and their respective molecular weights (23). According to the average ^{15}N-R_2, ~75% of the complex is present in the monomeric form. However, this is an underestimation of the amount of monomer in solution, because faster relaxation rates were observed for some residues. It is likely that these faster rates reflect a contribution from exchange broadening due to the monomer/dimer equilibrium. Without these residues (^{15}N-R_2 > 13 s^{-1}), the average ^{15}N-R_2 decreased significantly to 10.4 ± 1.7 s^{-1} (59 peaks). This indicates that >85% of the complex is in the monomeric form, which is consistent with the ratio of the peak intensities for the twin peaks identified above that result from the monomer/dimer equilibrium in solution. Overall, the ^{15}N-R_2 relaxation data per residue show the typical characteristics of a folded protein, which indicates that the structure of the N-domain is not perturbed by the presence of the probe. The relaxation rates for residues at the extremities of the sequence were smaller, as is typical for the flexible terminal regions. The relaxation rates observed for residues 56–63 of the C-helix were similar, but slightly higher, compared to those measured for the other secondary structures with an average ^{15}N-R_2 of 12.5 s^{-1}. Therefore, the C-helix is not perturbed, and is certainly not more flexible with the more rigid BSR probe attached.

Ca^{2+}-regulation of isometric force in muscle fibers

The isometric force produced by single demembranated fibers from rabbit psoas muscles at saturating [Ca^{2+}] was reduced by replacement of native sTnC by BR- or BSR-labeled

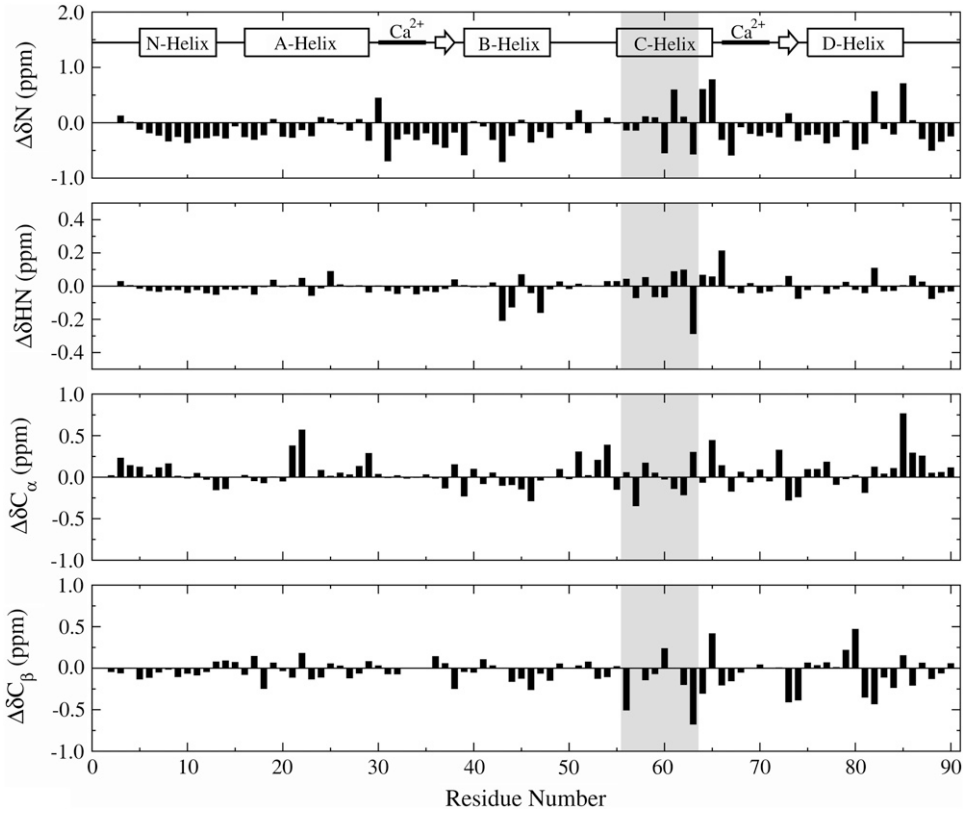

FIGURE 4 Difference in ^{15}N, ^{1}HN, $^{13}C\alpha$, and $^{13}C\beta$ chemical shifts between sNTnC·2Ca^{2+}·$TnI_{115–131}$·$BSR_{56–63}$ and sNTnC·2Ca^{2+}·$TnI_{115–131}$·$BR_{56–63}$. The gray area corresponds to the region of the N-domain where the bifunctional rhodamine label is attached. The resonances with higher intensity were chosen for twin peaks.

recombinant sTnC. After introduction of sTnC·BR, sTnC·BSR1, and sTnC·BSR2, isometric force was 82 ± 6% (mean ± SE, $n = 5$), 77 ± 2% ($n = 4$), and 64 ± 6% ($n = 4$), respectively, of the pre-exchange value in each fiber (Table 1). The mean value for sTnC·BR is similar to that reported previously for unlabeled recombinant sTnC (3,24). Isometric force also developed more slowly in fibers containing sTnC·BR, sTnC·BSR1, or sTnC·BSR2 than in control fibers (Table 1). As with maximum isometric force, modification of fiber function appears to be greater for BSR than BR, and greater for BSR2 than BSR1.

The Ca^{2+} sensitivity of isometric force was also reduced by the introduction of the labeled sTnCs (Fig. 7). The isometric force at each [Ca^{2+}] was expressed as a fraction of

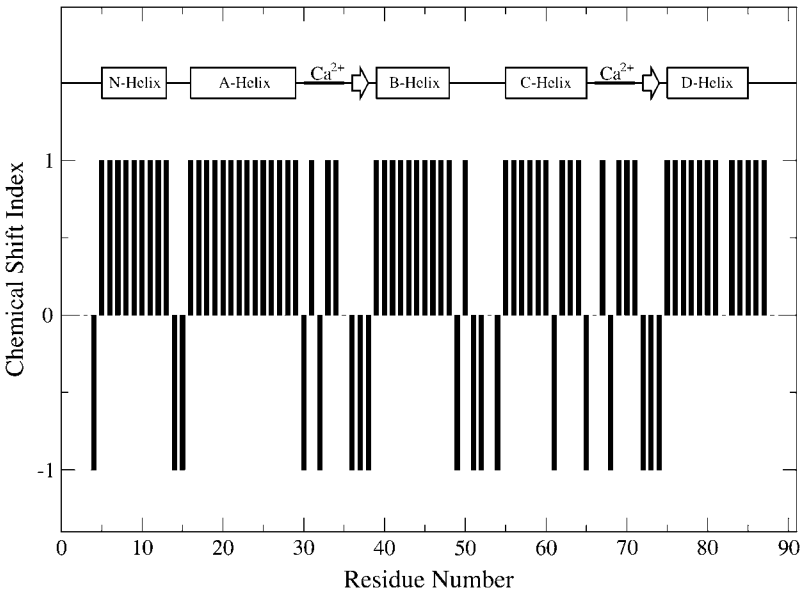

FIGURE 5 Secondary structure prediction of sNTnC·2Ca^{2+}·$TnI_{115–131}$·$BSR_{56–63}$ based on $^{13}C\alpha$ NMR chemical shift homology using the program Chemical Shift Index. The deviation of the Cα chemical shift from its random coil value is evaluated by the program: a value of +1 is assigned for the residues with a chemical shift characteristic of α-helices, 0 for random coil, and −1 for β-sheets. The secondary structure of sNTnC is the following: N-helix (D5–L13), A-helix (E16–F29), B-helix (T39–M48), C-helix (K55–V65), D-helix (F75–Q85), and small β-sheets (D36–S38 and T72–D74).

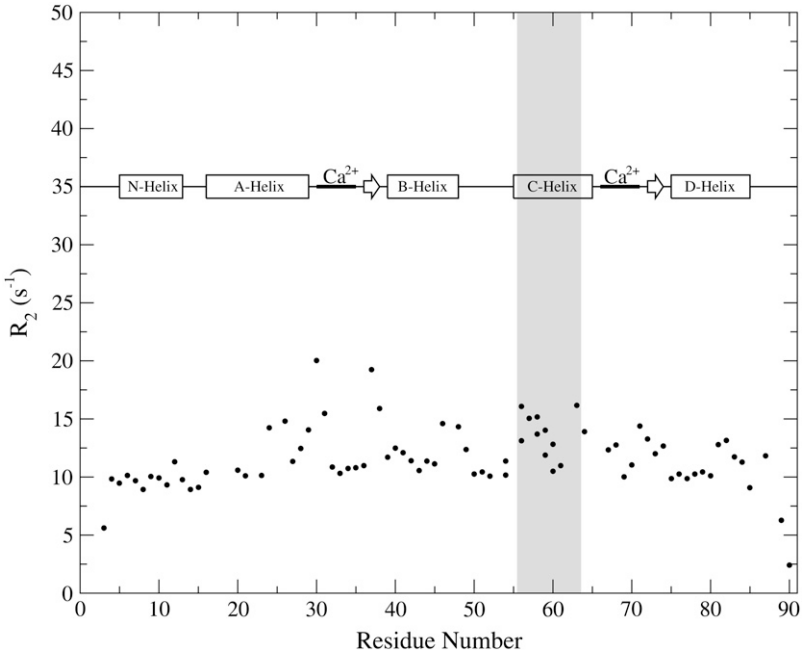

FIGURE 6 Backbone amide ^{15}N-R_2 NMR relaxation rates for each residue of sNTnC·2Ca^{2+}·$TnI_{115–131}$·$BSR_{56–63}$ at 600 MHz. The gray area corresponds to the region of the N-domain where the bifunctional rhodamine label is attached. Two separate values were calculated for the twin peaks (residues 54, 56, 58, 59, and 60).

maximum Ca^{2+}-activated force at pCa 4.5, plotted against pCa, and fitted with the Hill equation (see Methods). The pCa value that produced half-maximum force (pCa_{50}) was reduced after introduction of sTnC·BR (*squares*), sTnC·BSR1 (*triangles*), or sTnC·BSR2 (*diamonds*) by 0.40, 0.70, and 1.02 units, respectively (Table 1). A preliminary Ca^{2+} titration of sNTnC·$BSR_{56–63}$ in solution supports the conclusion that the BSR probe reduces the Ca^{2+} affinity of TnC (see Supplementary Material). The steepness of the force-pCa relationship (indicated by the Hill coefficient, n_H) in fibers containing sTnC·BR, sTnC·BSR1, or sTnC·BSR2 was similar to that measured in control fibers before sTnC exchange.

Orientation of the rhodamine dipoles on TnC in muscle fibers

The orientations of the BR and BSR probes on sTnC incorporated into muscle fibers were determined by polarized fluorescence measurements and expressed in terms of the order parameters $\langle P_{2d}\rangle$, $\langle P_2\rangle$, and $\langle P_4\rangle$ (3,19). $\langle P_{2d}\rangle$ describes the amplitude of the local rotation of the rhodamine dipole with respect to the protein backbone. $\langle P_{2d}\rangle$ was independent of [Ca^{2+}] and close to 0.91 for each of the three rhodamine-labeled sTnCs (Table 1). This value corresponds to that expected for uniform wobble in a cone of semiangle 20° on a timescale that is short compared with the fluorescence lifetime. There were no significant differences between $\langle P_{2d}\rangle$ values for BR- and BSR-labeled sTnC, or between those for the two diastereoisomers of sTnC·BSR. These results suggest that, once attached to the C-helix of TnC in a muscle fiber, there is no difference in the fast local motion of the BR and BSR probes relative to the protein backbone. Preliminary measurements of the excited-state lifetime of sTnC·BR and sTnC·BSR in isolated muscle fibers revealed no substantial difference between the lifetimes of the two probes in situ; both had values of ~4 ns.

The order parameters $\langle P_2\rangle$ and $\langle P_4\rangle$ describe the orientation distribution of the BR and BSR dipoles with respect to the muscle fiber axis, averaged over a timescale that is long compared with the fluorescence lifetime, and with the rapid local motion of the probes factored out. Formally, they correspond to the second- and fourth-rank coefficients of the Legendre polynomial expansion of this orientation distribution. $\langle P_2\rangle$ would be +1 if all the dipoles were parallel to the fiber axis, and −0.5 if they were all perpendicular to that axis. $\langle P_4\rangle$ gives orientation information at higher resolution. There were reproducible differences between the $\langle P_2\rangle$ and $\langle P_4\rangle$ values for the different labeled sTnCs (Table 1 and Fig. 8), indicating differences between the orientation distributions of the BR and BSR dipoles with respect to the fiber axis.

For all three rhodamine labeled sTnCs, $\langle P_2\rangle$ decreased substantially when the muscle fibers were activated (Fig. 8 *A*), signaling a large increase in the angle between the rhodamine dipole and the fiber axis, as reported previously for sTnC·BR (3). $\langle P_4\rangle$, in contrast, showed different behavior for the three probes (Fig. 8 *B*). The Ca^{2+} dependence of the changes in $\langle P_2\rangle$ and $\langle P_4\rangle$ were analyzed using the Hill equation (fitted curves in Fig. 8). The $\langle P_2\rangle$ data are more reliable as the signal/noise ratio is greater. The pCa_{50} for $\langle P_2\rangle$ was similar to that for force for each labeled sTnC. The $\langle P_2\rangle$-Ca^{2+} relationship was steeper for sTnC·BSR2 than for sTnC·BSR1 (Table 1). These results confirm the conclusion from the force-Ca^{2+} relationship (Fig. 7), that the introduction of the rhodamine labels on the C-helix of sTnC reduces the Ca^{2+} affinity of the regulatory sites, and that this effect is larger for BSR than BR.

TABLE 1 Fiber force and fluorescence polarization measurements

	pCa	sTnC·BR ($n = 5$)	sTnC·BSR1 ($n = 4$)	sTnC·BSR2 ($n = 4$)
			Isometric force	
Peak force (%)†		81.5 ± 5.8	77.3 ± 1.9^{ns}	64.2 ± 6.4$^{ns\ (ns)}$
Half time of force rise (%)†		189 ± 25	293 ± 43*	420 ± 62**$^{(ns)}$
pCa_{50} for force		6.00 ± 0.08	5.70 ± 0.04*	5.38 ± 0.03***$^{(***)}$
n_H for force		2.71 ± 0.18	2.80 ± 0.82^{ns}	2.95 ± 0.23$^{ns\ (ns)}$
			Order parameters	
$\langle P_{2d}\rangle$	9.0	0.915 ± 0.015	0.926 ± 0.024^{ns}	0.922 ± 0.009$^{ns\ (ns)}$
$\langle P_{2d}\rangle$	4.5	0.895 ± 0.013	0.911 ± 0.019^{ns}	0.921 ± 0.008$^{ns\ (ns)}$
$\langle P_2\rangle$	9.0	0.422 ± 0.021	0.471 ± 0.005^{ns}	0.396 ± 0.004$^{ns\ (***)}$
$\langle P_2\rangle$	4.5	−0.126 ± 0.006	−0.079 ± 0.019*	−0.004 ± 0.014***$^{(*)}$
$\langle P_4\rangle$	9.0	0.128 ± 0.027	0.016 ± 0.011**	−0.031 ± 0.005***$^{(**)}$
$\langle P_4\rangle$	4.5	−0.012 ± 0.021	0.005 ± 0.021^{ns}	0.000 ± 0.006$^{ns\ (ns)}$
pCa_{50} for $\langle P_2\rangle$‡		6.02 ± 0.03	5.59 ± 0.07***	5.37 ± 0.02***$^{(***)}$
n_H for $\langle P_2\rangle$‡		1.94 ± 0.15	2.21 ± 0.38^{ns}	3.32 ± 0.33**$^{(ns)}$
			Gaussian fitting	
θ_g (°)	9.0	34.6 ± 1.9	34.9 ± 0.3^{ns}	38.2 ± 0.2$^{ns\ (***)}$
θ_g (°)	4.5	67.2 ± 2.3	64.6 ± 1.4^{ns}	62.2 ± 1.1$^{ns\ (ns)}$
σ (°)	9.0	26.0 ± 1.3	16.4 ± 0.4***	17.4 ± 0.2***$^{(ns)}$
σ (°)	4.5	22.4 ± 2.8	26.0 ± 1.6^{ns}	28.0 ± 0.8$^{ns\ (ns)}$
θ_f (°)	9.0	36.2 ± 0.9	35.0 ± 0.3^{ns}	38.3 ± 0.2$^{ns\ (***)}$
θ_f (°)	4.5	63.3 ± 0.5	61.3 ± 1.0^{ns}	57.9 ± 0.4***$^{(*)}$
			Maximum entropy	
θ_{ME} (°)	9.0	36.8 ± 1.1	35.0 ± 0.2^{ns}	38.3 ± 0.2$^{ns\ (**)}$
θ_{ME} (°)	4.5	63.0 ± 0.3	60.9 ± 1.0^{ns}	57.2 ± 0. 7***$^{(*)}$

All statistics are given as mean ± SE. The asterisks denote significance level in *t*-tests. *, $P < 0.05$; **, $P < 0.01$; ***, $P < 0.001$; ns, $P > 0.05$. Comparisons are with the relevant value for sTnC·BR. The superscripts in brackets are for comparisons between sTnC·BSR1 and sTnC·BSR2.
At pCa 4.5, the Gaussian model failed to fit $\langle P_2\rangle$ and $\langle P_4\rangle$ for two of the fibers containing sTnC·BR and one of the fibers containing sTnC·BSR1, so fitted parameters are for $n = 3$ in each case.
†Relative to fibers before TnC exchange for which the half-time of force development was 0.38 ± 0.03 s ($n = 19$), pCa_{50} was 6.40 ± 0.04 ($n = 5$) and n_H was 2.62 ± 0.40 ($n = 17$).
‡From data in Fig. 8 *A*.

The angle (θ) between the probe dipole and the muscle fiber axis was estimated from the measured $\langle P_2\rangle$ and $\langle P_4\rangle$ values for each probe by two independent methods: Gaussian model fitting (3) and maximum entropy analysis (20). In contrast to previous analyses (3), the distribution was not truncated at either $\theta = 0°$ or $\theta = 90°$ (see Materials and Methods, and Fig. 9 *A*), thus providing a more realistic representation of the orientation distribution in the molecular coordinate frame. The fitted Gaussian distribution for sTnC·BR (Fig. 9 *A*, *solid line*) in relaxed muscle fibers at pCa 9 had $\theta_g = 34.6 \pm 1.9°$ (mean ± SE, $n = 5$) and standard deviation (σ) 26.0 ± 1.3° (Table 1). The value of θ_g is larger than that reported previously (28°) using a Gaussian model distribution that was truncated at 0° (3). The fitted full Gaussian distributions for sTnC·BSR1 (Fig. 9 *A*, *dashed line*) and sTnC·BSR2 (*dotted line*) at pCa 9 had θ_g values of 34.9 ± 0.3° and 38.2 ± 0.2°, which are not significantly different from that for sTnC·BR. However, the distributions for the BSR probes are narrower than that for the BR probe; σ values for sTnC·BSR1 and sTnC·BSR2 were 16.4 ± 0.4° and 17.4 ± 0.2°, respectively (Table 1).

The maximum entropy distribution (f_{ME}) of axial angles (θ) (Fig. 9 *B*) is the broadest orientation distribution consistent with the observed $\langle P_2\rangle$ and $\langle P_4\rangle$ values, calculated by maximizing the informational entropy defined as $-f_{ME}.\ln f_{ME}$ (20). The maximum entropy distribution is necessarily symmetrical around $\theta = 90°$, and is plotted in Fig. 9 *B* only for the region $0° < \theta < 90°$. The f_{ME} distributions for relaxed muscle

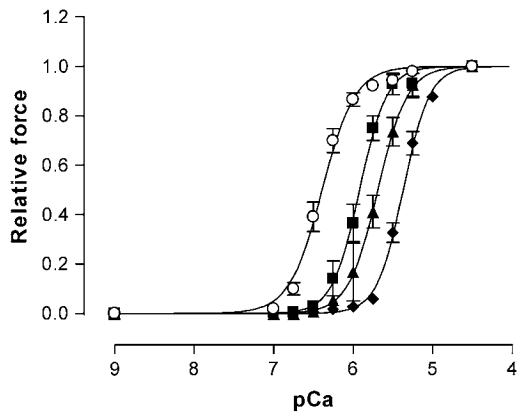

FIGURE 7 The Ca^{2+} dependence of force in control fibers (*circles*), fibers reconstituted with sTnC·BR (*squares*), or sTnC·BSR (sTnC·BSR1 (*triangles*) and sTnC·BSR2 (*diamonds*)). All data are scaled to the value obtained at pCa 4.5 for each labeled sTnC. Each point is the mean ± SE. Data were fitted to the mean data points with the Hill equation (see Methods).

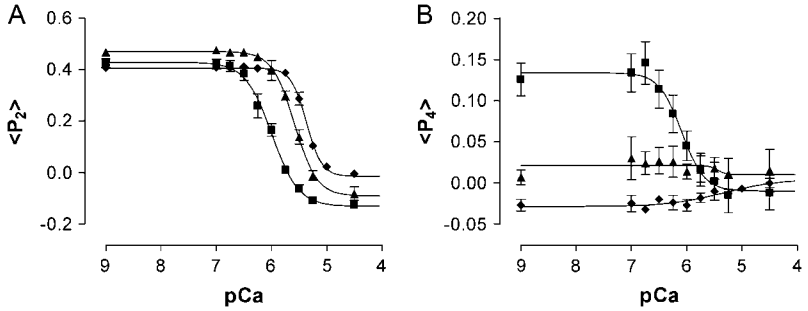

FIGURE 8 Ca^{2+} dependence of dipole order parameters $\langle P_2 \rangle$ and $\langle P_4 \rangle$ for sTnC·BR (*squares*) and the two diastereoisomers of sTnC·BSR (sTnC·BSR1 (*triangles*) and sTnC·BSR2 (*diamonds*)). Values are mean ± SE. Data were fitted to the mean data points with the Hill equation (see Methods).

fibers at pCa 9 for sTnC·BR (*solid line*), sTnC·BSR1 (*dashed line*), and sTnC·BSR2 (*dotted line*) are centered on about the same axial angle, but the f_{ME} distribution for BR is broader than that for either of the BSR isomers. The mean angles of these distributions (θ_{ME}) were 36.8 ± 1.1°, 35.0 ± 0.2°, and 38.3 ± 0.2° for sTnC·BR, sTnC·BSR1, and sTnC·BSR2, respectively (Table 1), and each of the θ_{ME} values is close to the respective peak (θ_g) value for the Gaussian model distributions (Fig. 9 *A*).

The maximum entropy (f_{ME}) and Gaussian (f_G) distributions can be compared more directly by noting that the cylindrical and bipolar sarcomere symmetry of the muscle fibers, combined with the dipolar nature of the probes, effectively folds the $\theta < 0°$ and $\theta > 90°$ tails of the molecular Gaussian distribution (Fig. 9 *A*) into the region $0° < \theta < 90°$, yielding the fiber-level orientation distribution shown in Fig. 9 *C*.

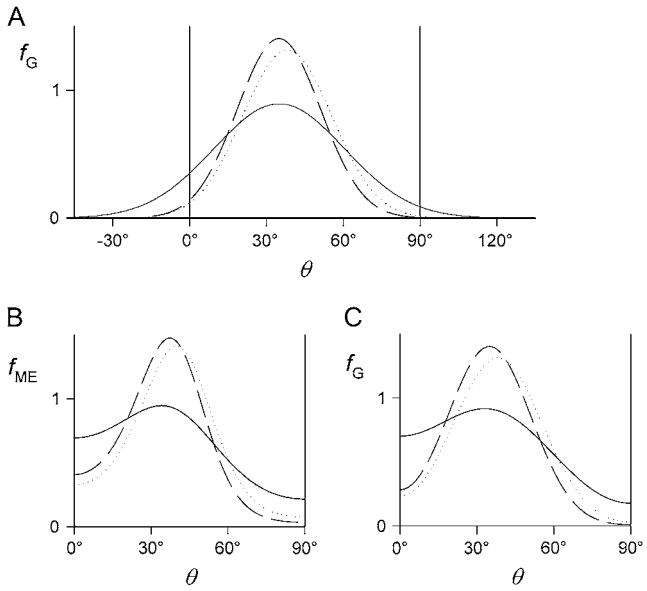

FIGURE 9 Distributions of angles θ between the bifunctional rhodamine dipole and the fiber axis in relaxed muscle, calculated from the mean $\langle P_2 \rangle$ and $\langle P_4 \rangle$ values for pCa 9 in Table 1 for sTnC·BR (*solid line*) and the two diastereoisomers of sTnC·BSR (sTnC·BSR1 (*dashed line*) and sTnC·BSR2 (*dotted line*)). All distributions have been normalized to unit area. (*A*) Gaussian distribution f_G crossing quadrant boundaries at $\theta = 0°$ and 90°. (*B*) One-dimensional maximum entropy distribution f_{ME}. (*C*) Folded Gaussian distribution confined to the region $0° < \theta < 90°$.

This ''folded Gaussian distribution'' no longer has a Gaussian shape; rather, it is similar in shape to the maximum entropy distribution f_{ME} (Fig. 9 *B*). The means (θ_f) of the folded Gaussian distributions for sTnC·BR, sTnC·BSR1, and sTnC·BSR2 were 36.2 ± 0.9°, 35.0 ± 0.3°, and 38.3 ± 0.2°, respectively (Table 1), very close to the corresponding θ_{ME} values. The greater width of the distribution for the BR probe is again apparent in the folded Gaussian distributions (Fig. 9 *C*).

The Gaussian and maximum entropy analyses were also applied to the $\langle P_2 \rangle$ and $\langle P_4 \rangle$ values obtained for each probe during active isometric contraction (pCa 4.5; Table 1). θ_g was slightly larger than θ_f and θ_{ME} for each probe at pCa 4.5, but in each case θ_f was very close to θ_{ME}, as observed at pCa 9. All three angles were smaller for sTnC·BSR2 than for sTnC·BSR1, and smaller for sTnC·BSR1 than for sTnC·BR. These differences support the evidence from isometric force measurements (Fig. 7 and Table 1) that fibers containing sTnC·BSR2 and, to a lesser extent, those containing sTnC·BSR1, may not be fully activated at pCa 4.5. The same phenomenon is probably responsible for the slightly larger value of σ observed for the BSR probes during active contraction (Table 1); incomplete activation at pCa 4.5 of fibers containing the BSR probes would lead to a population of TnC molecules in the relaxed orientation, thereby increasing the measured orientational dispersion.

DISCUSSION

The experiments described above compared a wide range of properties of two cysteine-directed bifunctional fluorescent probes, BR-I_2 and BSR-I_2, that were used to label the same protein, namely, the C-helix of sTnC. The results lead to specific conclusions about the efficacy of these two particular probes for determining the orientation of sTnC in muscle fibers. The comparison of the results from the two probes also allows some more general conclusions to be drawn about the power and limitations of the bifunctional fluorophore approach for determining the structure and orientation of protein domains in the cellular environment.

BSR-I_2 was found to react much more rapidly than BR-I_2 with the pair of cysteine residues introduced into sTnC at positions 56 and 63. The greater reactivity of BSR-I_2 is a

significant advantage for the convenient production of the desired conjugate, in which the probe cross-links the target cysteines, at the required purity. A similar difference in reactivity between BSR-I_2 and BR-I_2 has been observed for the E8C/L15C, K11C/Q73C, and P70C/N77C mutants of the A2 isoform of the essential light chain of chicken skeletal myosin (25). The difference in cysteine-directed reactivity between BSR-I_2 and BR-I_2 is therefore likely to be a general property of these reagents, which may be due to stereo-electronic influences within the piperazine rings of BSR-I_2 that enhance the reactivity of its iodoacetamido groups.

The native structure of the N-domain of sTnC is not significantly affected by BSR attached to residues E56C and E63C of its C-helix. The backbone chemical shifts of sNTnC·$BSR_{56–63}$ are similar to those of sNTnC·$BR_{56–63}$, even for the C-helix region. The identification of protein secondary structure using Cα chemical shifts indicates the formation of five α-helices and a small β-sheet. The relaxation data obtained for sNTnC·$2Ca^{2+}$·$TnI_{115–131}$·$BSR_{56–63}$ are equivalent to those for sNTnC·$2Ca^{2+}$·$TnI_{115–131}$·$BR_{56–63}$, demonstrating that, like the BR probe (7), the BSR probe does not significantly affect the conformation of the C-helix or the overall dynamics of the protein in solution.

Both sTnC·BR and sTnC·BSR were able to support Ca^{2+} regulation of contraction when exchanged into demembranated muscle fibers, but the mean isometric force at pCa 4.5 was smaller for sTnC·BSR than for sTnC·BR, suggesting that fibers containing sTnC·BSR were not fully activated at pCa 4.5. The rate of force development upon transferring fibers from pCa 9 to pCa 4.5 was also lower for sTnC·BSR than for sTnC·BR, and lower for sTnC·BSR2 than for sTnC·BSR1. In each case, the rate was lower than in control fibers. These changes in activation kinetics were correlated with the observed changes in Ca^{2+} sensitivity, as indicated by both isometric force and the orientation changes reported by polarized fluorescence. In each case, the change was greater for BSR than for BR, and larger for BSR2 than for BSR1. Thus, although the secondary structure of TnC is not affected by BR- or BSR-labeling, the Ca^{2+} affinity and binding kinetics of the regulatory sites in the N lobe of sTnC are affected, presumably as a direct result of the proximity of the probes to the Ca^{2+}-binding sites. Different Ca^{2+} affinities for the two diastereoisomers of sTnC·BSR might be explained by different orientations of the electric dipole of BSR with respect to the protein. The calculated electric dipole for a carborhodamine such as in BR is 19 Debye, oriented at ~40° to the plane of the xanthene ring (21). It would have a similar orientation in a sulforhodamine such as BSR, although the more diffuse charge distribution on the sulfonate may somewhat modify its magnitude. Because the orientation of the dipole depends on the position of the sulfonate group (above or below the plane of the xanthene ring), the dipole's orientation relative to the protein will differ between the two diastereoisomers by ~80°, assuming the xanthene ring of the BSR has the same orientation in the two diastereosiomers. Much smaller modulations of electric dipoles (changes $\leq$ 3 Debye) have been shown to have significant effects on the ion channel gating of modified gramicidin (26,27). Since the more rigid BSR probe is likely to hold the dipole of the two diasteroisomers in more defined orientations relative to the protein than is the case for the diastereoisomers of the more flexible BR probe, it is at least feasible that the observed differences in Ca^{2+} affinity of the sNTnC·BSR diastereoisomers could be attributed to this differential electric dipolar effect.

The similarity of the observed values of the order parameter $\langle P_{2d} \rangle$ for sTnC·BSR and sTnC·BR in muscle fibers shows that the amplitude of the local orientational motion of the rhodamine fluorescence dipole with respect to the protein backbone was similar for the two probes. $\langle P_{2d} \rangle$ for both probes corresponds to that expected for uniform wobble in a cone of semiangle ~20° on a timescale that is fast compared with the fluorescence lifetime, which is ~4 ns. The fact that the greater flexibility of the linkers between the probe dipole and cysteine attachments in BR does not result in a greater degree of independent rapid motion of the probe suggests that the BR probe is immobilized to some extent by an interaction with the protein surface.

The orientation of the BR and BSR dipoles with respect to the fiber axis was estimated from the order parameters $\langle P_2 \rangle$ and $\langle P_4 \rangle$ by two independent analytical approaches, based on fitting Gaussian orientation distributions and on maximum entropy analysis. The Gaussian fitting approach was modified from that used previously (1–3), in which the Gaussian fitting was applied in the fiber coordinate frame, and truncated at $\theta = 0°$ because negative values of θ are not defined in that frame. Here, we applied the Gaussian model in the molecular coordinate frame, in which there is no physical reason to exclude negative axial angles, so the distributions were not truncated at $\theta = 0°$. We then transformed this distribution into the fiber frame by folding the $\theta < 0°$ tail of the molecular-frame Gaussian into the $\theta > 0°$ region in the fiber frame. The bipolar symmetry of the muscle sarcomeres and the dipole nature of the probes impose additional mirror symmetry around $\theta = 90°$ in the fiber orientation distributions, and this symmetry was taken into account in previous Gaussian fitting analyses.

The maximum entropy distribution of axial probe angles is the broadest orientation distribution in the fiber coordinate frame that is consistent with the observed $\langle P_2 \rangle$ and $\langle P_4 \rangle$ values. It is defined only for positive θ, but has mirror symmetry around $\theta = 90°$. The maximum entropy distributions were similar to the folded Gaussian distributions for each probe in each condition studied here. The means of the two distributions in the region $0° < \theta < 90°$, θ_{ME}, and θ_f, respectively, were equal to within 1° in each case. The agreement of the mean angles derived from the model-independent maximum entropy analysis and the folded Gaussian analysis suggest that both methods give a reliable estimate of the orientation distribution of the probes in the fiber frame, at

least at the relatively low angular resolution implied by knowledge of only the first two second-rank order parameters, $\langle P_2 \rangle$ and $\langle P_4 \rangle$. The folded Gaussian analysis also suggests that these fiber-frame distributions result from Gaussian distributions in the molecular frame, at the same angular resolution. The isolation of these molecular orientation distributions, characterized by peak angle θ_g and standard deviation σ, is explicitly distinguished from orientation distributions in the fiber frame for the first time that we know of by the analysis described here.

Applying these general conclusions to the results of these experiments, the molecular-frame orientations of the sTnC·BR, sTnC·BSR1, and sTnC·BSR2 probes are defined by the Gaussian parameters θ_g and σ. The comparison of the parameters for the three probes is most informative for relaxed muscle fibers (pCa 9), in which all the TnC molecules in the fiber are in the ''off'' conformation. In these conditions, θ_g values for the sTnC·BR, sTnC·BSR1, and sTnC·BSR2 probes were almost equal, suggesting that the peak orientation of each of the probes accurately reports that of the C-helix residues to which they are attached. However, σ was significantly larger for sTnC·BR than for sTnC·BSR1 and sTnC·BSR2; as might be expected on the basis of the greater flexibility of the probe-protein linkers in the BR probe. In this context, it is important to note that σ is not related to the independent motion of the probes on timescales shorter than the ~4-ns fluorescence lifetime, which we have shown on the basis of the $\langle P_{2d} \rangle$ measurements is similar for the BR and BSR probes. The difference in σ rather suggests that the greater flexibility of BR allows the probe to adopt a wider range of conformations with respect to the protein backbone, but that motion between these conformations takes place on timescales longer than 4 ns. The value of σ observed for the less flexible BSR probe, ~17°, thus represents a probable upper limit for the standard deviation of the axial orientations of the C-helix of TnC in a relaxed muscle fiber.

The results presented here demonstrate the potential of polarized fluorescence measurements with bifunctional probes to measure the orientation of protein domains in their native environment with minimal disruption of native structure. They also illustrate the sensitivity of the measured orientational and functional parameters to probe chemistry. In the case of cysteines at positions 56 and 63 on the C-helix of sTnC, the bifunctional probes BR and BSR have complementary advantages and disadvantages. BSR has much greater reactivity for this pair of sites, and probably for all cysteine residues, and this facilitates the preparation of probe-protein conjugates at the required purity. Neither probe alters the structure of sTnC in solution, but both reduce the Ca^{2+} affinity of its regulatory sites and this effect is more pronounced for BSR than for BR. The extent of the reduction is different for the two diastereoisomers of sTnC·BSR. Both probes are likely to accurately report the mean in situ orientation of the vector joining the two cysteines to which they are attached.

SUPPLEMENTARY MATERIAL

To view all of the supplemental files associated with this article, visit www.biophysj.org.

We thank the Canadian National High Field NMR Centre (NANUC) for their assistance and use of their facilities.

Operation of NANUC is funded by the Canadian Institutes of Health Research, the Natural Science and Engineering Research Council of Canada, and the University of Alberta. The experiments in Edmonton were funded by the Canadian Institutes of Health Research, and the experiments in London were funded by the Medical Research Council, U.K. O.J. was supported by a studentship from Fonds de la Recherche en Santé du Québec.

REFERENCES

1. Corrie, J. E. T., B. D. Brandmeier, R. E. Ferguson, D. R. Trentham, J. Kendrick-Jones, S. C. Hopkins, U. A. van der Heide, Y. E. Goldman, C. Sabido-David, R. E. Dale, S. Criddle, and M. Irving. 1999. Dynamic measurement of myosin light-chain domain tilt and twist in muscle contraction. *Nature*. 400:425–430.
2. Hopkins, S. C., C. Sabido-David, U. A. van der Heide, R. E. Ferguson, B. D. Brandmeier, R. E. Dale, J. Kendrick-Jones, J. E. T. Corrie, D. R. Trentham, M. Irving, and Y. E. Goldman. 2002. Orientation changes of the myosin light-chain-domain during filament sliding in active and rigor muscle. *J. Mol. Biol.* 318:1275–1291.
3. Ferguson, R. E., Y. B. Sun, P. Mercier, A. S. Brack, B. D. Sykes, J. E. T. Corrie, D. R. Trentham, and M. Irving. 2003. *In situ* orientations of protein domains: troponin C in muscle fibers. *Mol. Cell.* 11:865–874.
4. Brack, A. S., B. D. Brandmeier, R. E. Ferguson, S. Criddle, R. E. Dale, and M. Irving. 2004. Bifunctional rhodamine probes of myosin regulatory light chain orientation in relaxed skeletal muscle fibers. *Biophys. J.* 86:2329–2341.
5. Forkey, J. N., M. E. Quinlan, M. A. Shaw, J. E. T. Corrie, and Y. E. Goldman. 2003. Three-dimensional structural dynamics of myosin V by single-molecule fluorescence polarization. *Nature*. 422:399–404.
6. Yildiz, A., J. N. Forkey, S. A. McKinney, T. Ha, Y. E. Goldman, and P. R. Selvin. 2003. Myosin V walks hand-over-hand: single fluorophore imaging with 1.5-nm localization. *Science*. 300:2061–2065.
7. Mercier, P., R. E. Ferguson, M. Irving, J. E. T. Corrie, D. R. Trentham, and B. D. Sykes. 2003. The NMR structure of a bifunctional rhodamine labeled N-domain of troponin C complexed with the regulatory 'switch' peptide from troponin I; implications for *in situ* fluorescence studies in muscle fibers. *Biochemistry*. 42:4333–4348.
8. Corrie, J. E. T., J. S. Craik, and V. R. N. Munasinghe. 1998.A homobifunctional rhodamine for labeling proteins with defined orientations of a fluorophore. *Bioconjug. Chem.* 9:160–167.
9. Peterman, E. J. P., H. Sosa, L. S. B. Goldstein, and W. E. Moerner. 2001. Polarized fluorescence microscopy of individual and many kinesin motors bound to axonemal microtubules. *Biophys. J.* 81:2851–2863.
10. Asenjo, A. B., N. Krohn, and H. Sosa. 2003. Configuration of the two kinesin motor domains during ATP hydrolysis. *Nat. Struct. Biol.* 10: 836–842.
11. Sykes, B. D., L. F. Saltibus, and L. Spyracopoulos. 1998. Checking pH without an electrode. *NMR Newsletter*. 479:11–12.
12. Johnson, B. A. 2004. Using NMRView to visualize and analyze the NMR spectra of macromolecules. *Methods Mol. Biol.* 278:313–352.
13. Delaglio, F., S. Grzesiek, G. W. Vuister, G. Zhu, J. Pfeifer, and A. Bax. 1995. NMRPipe: a multidimensional spectral processing system based on UNIX pipes. *J. Biomol. NMR*. 6:277–293.
14. Slupsky, C. M., R. F. Boyko, V. K. Booth, and B. D. Sykes. 2003. Smartnotebook: a semi-automated approach to protein sequential NMR resonance assignments. *J. Biomol. NMR*. 27:313–321.

15. Wishart, D. S., and B. D. Sykes. 1994. The 13C chemical-shift index: a simple method for the identification of protein secondary structure using 13C chemical-shift data. *J. Biomol. NMR.* 4:171–180.

16. Sabido-David, C., B. Brandmeier, J. S. Craik, J. E. T. Corrie, D. R. Trentham, and M. Irving. 1998. Steady-state fluorescence polarization studies of the orientation of myosin regulatory light chains in single skeletal muscle fibers using pure isomers of iodoacetamidotetramethylrhodamine. *Biophys. J.* 74:3083–3092.

17. Sun, Y.-B., B. D. Brandmeier, and M. Irving. 2006. Structural changes in troponin in response to Ca^{2+} and myosin binding to thin filaments during activation of skeletal muscle. *Proc. Natl. Acad. Sci. USA.* 103: 17771–17776.

18. Bell, M. G., R. E. Dale, U. A. van der Heide, and Y. E. Goldman. 2002. Polarized fluorescence depletion reports orientation distribution and rotational dynamics of muscle cross-bridges. *Biophys. J.* 83:1050–1073.

19. Dale, R. E., S. C. Hopkins, U. A. van der Heide, T. Marszalek, M. Irving, and Y. E. Goldman. 1999. Model-independent analysis of the orientation of fluorescent probes with restricted mobility in muscle fibers. *Biophys. J.* 76:1606–1618.

20. van der Heide, U. A., S. C. Hopkins, and Y. E. Goldman. 2000. A maximum entropy analysis of protein orientations using fluorescence polarization data from multiple probes. *Biophys. J.* 78:2138–2150.

21. Cavallo, L., M. H. Moore, J. E. T. Corrie, and F. Fraternali. 2004. Quantum mechanics calculations on rhodamine dyes require inclusion of solvent water for accurate representation of the structure. *J. Phys. Chem. A.* 108:7744–7751.

22. McKay, R. T., B. P. Tripet, J. R. Pearlstone, L. B. Smillie, and B. D. Sykes. 1999. Defining the region of troponin-I that binds to troponin-C. *Biochemistry.* 38:5478–5489.

23. Lindhout, D. An NMR investigation of Troponin-I within the cardiac troponin complex and the effects on calcium induced cardiac muscle contraction: the ''I'' in team. PhD Thesis. University of Alberta, Edmonton, Alberta, Canada.

24. Regnier, M., A. J. Rivera, P. B. Chase, L. B. Smillie, and M. M. Sorenson. 1999. Regulation of skeletal muscle tension redevelopment by troponin C constructs with different Ca^{2+} affinities. *Biophys. J.* 76: 2664–2672.

25. Knowles, A. C., R. E. Ferguson, B. D. Brandmeier, J. Kendrick-Jones, J. E. T. Corrie, D. R. Trentham, and M. Irving. 2004. Orientation of the essential light chain region of myosin in skeletal muscle fibers determined by polarized fluorescence. *Biophys. J.* 86:187a–188a.

26. Borisenko, V., D. C. Burns, Z. Zhang, and G. A. Woolley. 2000. Optical switching of ion-dipole interactions in a gramicidin channel analogue. *J. Am. Chem. Soc.* 122:6364–6370.

27. Lougheed, T., V. Borisenko, T. Hennig, K. Rück-Braun, and G. A. Woolley. 2004. Photomodulation of ionic current through hemithioindigo-modified gramicidin channels. *Org. Biomol. Chem.* 2: 2798–2801.